

Spin-valve-like magnetoresistance in a Ni-Mn-In thin film

Sandeep Agarwal,^{1,2} Baomin Wang,^{1,2,*} Huali Yang,^{1,2} Pravarthana Dhanapal,^{1,2} Yuan Shen,^{1,2} Junling Wang,³ Hailong Wang,⁴ Jianhua Zhao,⁴ and Run-Wei Li^{1,2,†}

¹CAS Key Laboratory of Magnetic Materials and Devices, Ningbo Institute of Materials Technology and Engineering, Chinese Academy of Sciences, Ningbo 315201, People's Republic of China

²Zhejiang Province Key Laboratory of Magnetic Materials and Application Technology, Ningbo Institute of Materials Technology and Engineering, Chinese Academy of Sciences, Ningbo 315201, People's Republic of China

³School of Materials Science and Engineering, Nanyang Technological University, 639798 Singapore

⁴State Key Laboratory of Superlattices and Microstructures, Institute of Semiconductors, Chinese Academy of Sciences, Beijing 100083, People's Republic of China



(Received 9 January 2018; revised manuscript received 24 May 2018; published 25 June 2018)

Spin valve devices, the resistive state of which is controlled by switching the magnetization of a free ferromagnetic layer with respect to a pinned ferromagnetic layer, rely on the scattering of electrons within the active medium to work. Here we demonstrate spin-valve-like effect in the Ni-Mn-In thin films, which consists of a ferromagnetic phase embedded in an antiferromagnetic matrix. Through transport and magnetic measurements, we confirm that scattering at the interfaces between the two phases gives rise to a unidirectional anisotropy and the spin-valve-like effect in this system. The magnitude of the spin-valve-like magnetoresistance (about 0.4% at 10 K) is stable within the temperature range of 10–400 K. The low- and high-resistance states cannot be destroyed even under a high magnetic field of 100 kOe. This finding opens up a way of realizing the spin valve effect in materials with competing ferromagnetic and antiferromagnetic interactions, where the interface between these phases acts as the active medium.

DOI: [10.1103/PhysRevB.97.214427](https://doi.org/10.1103/PhysRevB.97.214427)

I. INTRODUCTION

Conventional spin valves (SVs) used for magnetic sensing and recording require multilayers of magnetic materials to achieve the low- and high-resistance states [1–4]. These devices rely on spin-dependent scattering in the ferromagnetic (FM) layers to achieve the desired effect [5]. Recently, spintronic devices with antiferromagnets (AFMs) as the active layers have become an emerging field that holds great promise. They are less energy intensive, are scalable, are robust against the external perturbations, and possess an ultrafast dynamics, which make them ideal candidates for future spintronics. Such devices are made possible by the anisotropic magnetoresistance (AMR) effect present in AFMs [6,7] and recent breakthroughs in the control and detection of AFMs [8–11]. SV-like effect of about 0.03% has been observed in Mn₂NiGa crystals with a tetragonal structure at room temperature that shows little variation with the change in temperature [12]. The effect depends on the direction of the initially applied field irrespective of the sample being a single crystal or polycrystal. The SV-like effect in this system is the result of interfacial scattering at the FM/AFM boundaries. Better understanding of this effect will enable us to further enhance the SV-like effect in the system. Furthermore, realization of this effect in the thin films will make them practically more viable.

The Ni-Mn-*X* (*X* = In, Sn, Sb) system with low *X* concentration is known to possess mixed AFM/FM phases [13,14].

When the FM phase is embedded in an AFM matrix, exchange bias interaction is known to establish a unidirectional anisotropy (UA) in the system below the Neel temperature under both zero-field and field cooling conditions [15,16]. Such UA should also lead to different electrons scattering and two resistance states as shown in Figs. 1(a) and 1(b). In the present paper, we demonstrate such a SV-like effect in a Ni-Mn-In system. The SV-like magnetoresistance (MR) shows little variation against the temperature up to 400 K and is stable even after cooling under a 100-kOe field. The effect is almost ten times higher than that in the bulk Mn₂NiGa system [12].

II. EXPERIMENTAL METHOD

We have fabricated Ni-Mn-In thin films with low In concentrations using radio frequency sputtering with a base pressure of $<3 \times 10^{-7}$ Torr. The single-crystal MgO (001) substrate of 1×1 cm² was rotated during the deposition to get a homogeneous film. The sputtering was done under an Ar pressure of 6×10^{-3} Torr. Prior to the deposition, we heated the substrate to 773 K and maintained it for 10 min to make the temperature uniform. The Ni-Mn-In target was cleaned by presputtering with a closed shutter. Films were deposited for different time and annealed *in situ* at a temperature of 973 K after deposition. The samples were then cooled to room temperature *in situ*. The magnetic properties of the films were studied using a Quantum Design magnetic properties measurement system (Quantum Design's MPMS 3). The magnetotransport measurements were carried out using an Oxford Instrument 12 T (TeslatronPT) magnetic system fitted with a

* wangbaomin@nimte.ac.cn

† runweili@nimte.ac.cn

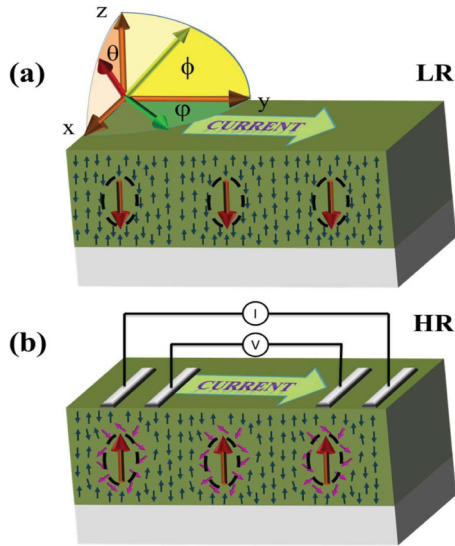


FIG. 1. The proposed device where the SV-like low resistance (LR) and high resistance (HR) states are obtained by applying a magnetic field without the requirement of an additional barrier or pinning layer. The perpendicular UA anisotropy is established due to the interface (pink arrow) between the FM region (marked by the red arrow in the dashed line) and AFM matrix (blue arrow) without multilayer fabrication. In panel (a) the sample coordinate used for the transport measurement is shown and panel (b) shows the four probe setup used for the transport measurement.

variable-temperature insert and a low-temperature rotator. The structure of the films was characterized using a Bruker D8 Discover high-resolution x-ray diffractometer (XRD). Field Electron and Ion (FEI) Quanta 250 field emission gun (FEG) integrated with the Oxford electron backscattering diffraction (EBSD) system controlled by Aztec Oxford data collection software was used to map the texture of the film.

III. RESULTS

A. Characterization and texture

The composition of the film was determined by energy dispersive x-ray analysis and confirmed to be $\text{Ni}_{52}\text{Mn}_{40}\text{In}_8$. The XRD result is shown in Fig. 2(a). The tetragonal structure alone was not sufficient to account for all the diffracted peaks in the system [17,18]; when double tetragonal structure was taken into account then all the diffracted peaks (hkl) could be indexed. The lattice parameters of 7.593 and 6.980 Å (≈ 0.92) agree well with those reported in the literature for similar compositions [17,18]. The film thickness was determined using the cross-sectional image and found to be 200 nm.

The intense peak observed at 50.9° corresponds to (330), and the peak at 61.4° corresponds to (430), which is 8.1° away from {110}. Presence of such an intense {110} diffraction peak indicates texturing along [110], which is confirmed by EBSD as shown in Fig. 2(b). The EBSD patterns were recorded over multiple regions of $40 \times 40 \mu\text{m}$ with a step size of 0.15 μm . These EBSD patterns were used to compute the orientation distribution function using Oxford Aztec analysis software. The computed texture in terms of orientation densities in the units of multiples of a uniform density (m.u.d.) represented in

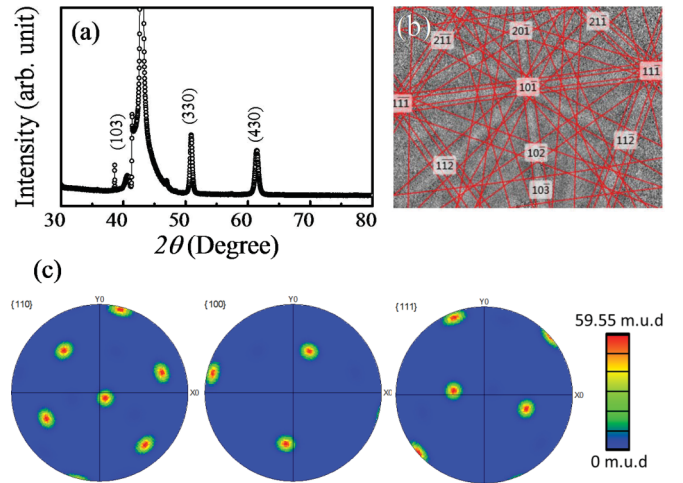


FIG. 2. (a) XRD Bragg pattern of the Ni-Mn-In film of thickness 200 nm deposited on MgO (001) single-crystal substrate. The Miller indices of the diffracted planes are indexed. (b) The indexed EBSD pattern of the Ni-Mn-In thin film. (c) Computed pole figure texture representation of (110), (100), and (111) planes in the Ni-Mn-In film from the EBSD measurements. The color coded legend of orientation density values of the pole figure in the unit of multiples of a uniform density (m.u.d.) from minimum to maximum is shown.

pole figures of (110), (100), and (111) is shown in Fig. 2(c). In a typical textured sample, the orientation density varies from 0 m.u.d. (absence of crystals oriented in this direction) to infinity (for a single crystal) [19]. In the current case, a brass $\{110\}\langle\bar{1}12\rangle$ type of texture is observed with maximum m.u.d. of 59.55 [20,21]. This is consistent with the XRD results, as well as previous work of Ni-Mn-In grown on MgO (001) by molecular-beam epitaxy [19].

B. Magnetic measurement

The magnetization-field (MH) loops are measured from 400 to 10 K [Fig. 3(a)]. The spontaneous magnetization is obtained by extrapolating the positive and negative high-field magnetization to zero internal magnetic field and taking the average [Fig. 3(b)] [22]. The curve above 10 K is fitted with the Brillouin function, $M = M_0(1 - \frac{T}{T_C})^\gamma$, leading to a Curie temperature (T_C) of 470 K with $\gamma = 0.14$ [23].

We have also performed MH measurements at 300 K for $\theta = 0, 45, \text{ and } 90^\circ$ as shown in Fig. 3(c) (diamagnetic contributions from the quartz sample holder and substrate were subtracted from all the data). The curves show that the easy axis lies along the in-plane direction. The spontaneous magnetization at zero internal magnetic field is lowest for $\theta = 45^\circ$. Also the curve at 45° shows higher slope above the saturation magnetization, suggesting that the AFM matrix in the sample is possibly aligned along 45°. Previous neutron-diffraction studies show that Mn moments in Ni-Mn are ordered antiferromagnetically either along [100] or [110] directions in the ab plane [24–26]. In the present case, it appears that the presence of In favors the AFM alignment along [100] (discussed in the following section). The [110] out-of-plane texture of the film thus means that the AFM matrix is at 45° as shown in Fig. 3(d). Since there is no in-plane texturing, the AFM matrix is randomly

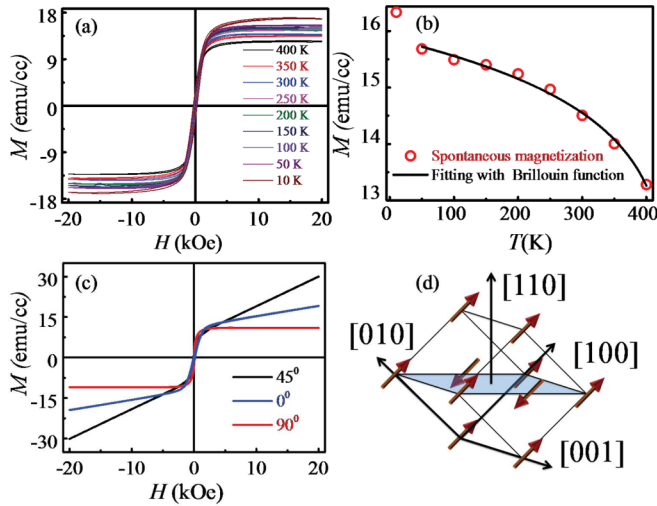


FIG. 3. (a) Isothermal magnetization measured at different temperatures; the diamagnetic contribution has been subtracted. (b) Spontaneous magnetization (red circle) calculated from panel (a) by extrapolating the high magnetic field part to the zero internal magnetic field and the fitting with the Brillouin function (black line) above 10 K which yielded the Curie temperature of 470 K. (c) Isothermal magnetization curve measured at 300 K for the magnetic field at $\theta = 0, 45,$ and 90° . (d) The out-of-plane (110) cell which exhibits AFM in the ab plane with spin along the [100] direction.

distributed along the surface of a cone with 45° angle. The magnetization measurement at 10 K after cooling under 5-T field does not show any exchange bias effect, indicating that the magnetic clusters in the film are of the order of a few nanometers as reported previously [12,27,28].

C. Temperature-dependent magnetoresistance

Longitudinal resistance was measured using the standard four-probe technique as schematically shown in Fig. 1(a). The contacts were made on the thin strip of the sample using epoxy silver paste and platinum wires. The current of 1 mA was driven through the outer contacts using a current source and the voltage was measured using the inner contacts. MR is defined as $[\rho(H) - \rho_0]/\rho_0$, where $\rho(H)$ is the resistance under a magnetic field H , and ρ_0 is the zero-field resistance. The MR curves obtained at different temperatures between 400 and 10 K are shown in Fig. 4(a). The current flowed in the y direction and the magnetic field was applied along the z axis. The sample displays SV-like asymmetric MR (AsyMR) within the entire temperature range. The MR curve in the low-field region changes at lower temperatures and shows the feature of a SV-like behavior and a peaklike MR with hysteresis as observed in a typical FM sample [inset of Fig. 4(a)]. The asymmetry results from the difference in the scattering at the FM/AFM interfaces [12]. Unlike the Mn_2NiGa system, in the present case the direction of asymmetry is fixed and independent of direction of the initially applied field [12].

In order to better understand the evolution of MR with temperature, we extract the AsyMR from Fig. 4(a), which has been defined as $(\text{MR}_{H+} - \text{MR}_{H-})/2$ as shown in Fig. 4(b). The asymmetry increases with increasing magnetic field and decreases at higher temperatures. The maximum value of

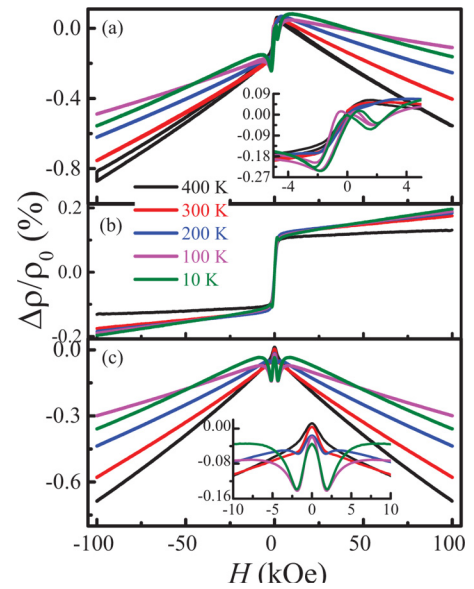


FIG. 4. Temperature dependence of the spin-valve-like MR. (a) Isothermal magnetoresistance of the sample measured for the current flowing in the y direction while applying the magnetic field in the z direction as shown in Fig. 1(a) for different temperatures; for the sake of clarity, not all MR curves are shown. The inset in panel (a) shows the magnified view in the low-field region. Symmetric (SymMR) and asymmetric (AsyMR) MR evaluated from panel (a) is shown in panels (b) and (c), respectively. The inset in panel (c) shows the magnified view around the low-field region.

AsyMR is $\sim 0.4\%$ at 10 K. Unlike conventional SV effect, where asymmetry vanishes under strong fields [2–4], we observe an asymmetry even under a magnetic field of 100 kOe. The AsyMR saturates under a field of 2.5 kOe, close to the magnetic saturation field, beyond which it increases relatively faster at 10 K compared to at 400 K. The increase in the AsyMR at low temperatures may arise from an increase in the mean free path which makes it more probable for electrons to get scattered by the FM/AFM interfaces. It is also possible that the transverse resistivity due to Hall effect contributes to asymmetric MR. However, identical contacts made on magnetic and nonmagnetic samples did not display any AsyMR. Furthermore, we performed the same measurements on several nontextured films of similar composition and thickness, using similar contact geometry. The MR in the nontextured films was found to be symmetric. This eliminates the possibility of contribution coming from the transverse resistivity. Moreover we find that the texture of the film is vital in obtaining the SV-like MR.

We also extract the symmetric MR (SymMR) from Fig. 4(a), which is defined as $(\text{MR}_{H+} + \text{MR}_{H-})/2$ as shown in Fig. 4(c). It shows peaklike feature at low magnetic fields for all temperatures. The peaklike feature of SymMR is completely overshadowed by the AsyMR for temperature ≥ 200 K in the MR curve. Below 300 K, the SymMR shows a rapid negative trend in the low-field region up to 2 kOe, followed by a slight positive trend till 7.5 kOe, beyond which it is again dominated by the negative MR as the field is increased [inset of Fig. 4(c)]. The positive MR increases as the temperature is lowered, because of the contribution from the fluctuating spins in the

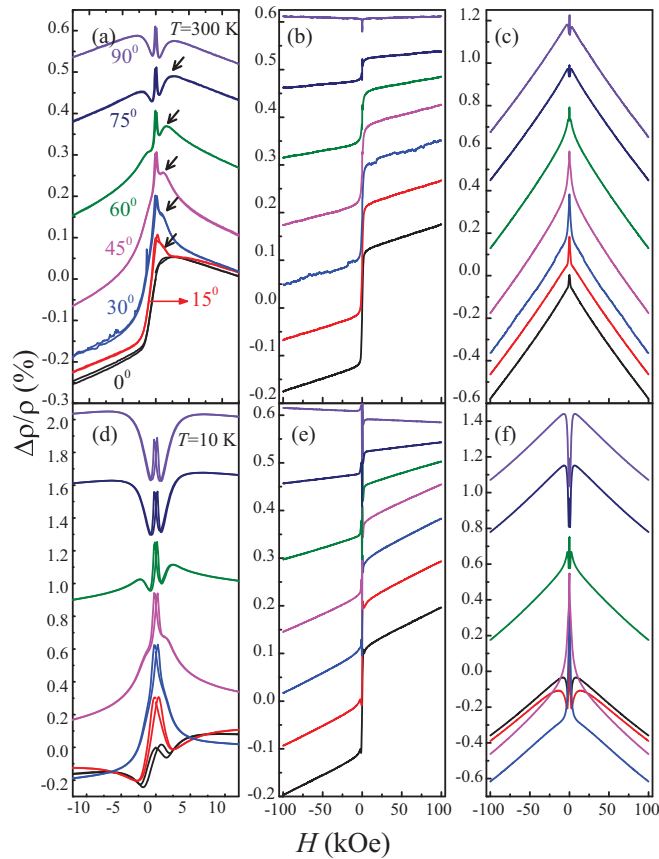


FIG. 5. Angle dependence of the spin-valve-like MR. (a) Magnetoresistance measured by changing the angle θ [defined in Fig. 1(a)] of the magnetic field (current flowing in the y direction) at 300 K. The curves display the SV-like MR for the magnetic field in the out-of-plane direction which diminishes as the field moves towards the in-plane direction. The curves are shown between ± 12.5 kOe, while the measurements were performed between ± 100 kOe. For the sake of clarity, the curves for the adjacent angles have been offset by 0.1% of $\Delta\rho/\rho_0$. SymMR and AsyMR evaluated from panel (a) are shown in panel (b) and (c), respectively. For the sake of clarity, the curves for adjacent angles have been offset by 0.1 and 0.2% of $\Delta\rho/\rho_0$. (d) The MR measured at 10 K under the same condition as panel (a). For the sake of clarity, the curves for the adjacent angles have been offset by 0.3% of $\Delta\rho/\rho_0$. SymMR and AsyMR evaluated from panel (d) are shown in panels (e) and (f), respectively. For the sake of clarity, the curves for the adjacent angles have been offset by 0.1 and 0.2% of $\Delta\rho/\rho_0$.

AFM matrix. Similar behavior has been observed in the case of the Ni-Mn-Ga system [29]. The negative MR observed at high temperatures and high magnetic fields is almost linear. This can be explained by the s - d scattering model [30]. The negative MR decreases at low temperatures as the contribution from s - d scattering dies down [29–31].

D. Angle dependence of magnetoresistance

To further understand the AsyMR behavior of the film, we performed MR measurements by changing the angle θ of the magnetic field, from 0 to 90° perpendicular to the current direction at 300 and 10 K [Figs. 5(a) and 5(d)]. As the θ

increases and the magnetic field moves towards the in-plane direction, we observe that the SV-like behavior diminishes and the MR curves become increasingly more symmetric. Interestingly, at 300 K, when θ is increased slightly, we see that a peaklike feature appears around zero field, which becomes stronger as the field moves towards the in-plane direction. Furthermore, as θ increases from 0 to 45°, MR decreases and beyond 45° it increases again till 90°. Another interesting observation is that, for small θ , the MR curve under the low magnetic field region is different for the positive and negative fields. A slight positive trend in MR is observed for positive (out of the plane) field which is absent in the case of negative (into the plane) field [marked by arrows in Fig. 5(a)]. This shows that, apart from asymmetry, there is an additional contribution to the scattering under positive field. The positive trend indicates that this contribution also comes from the spin fluctuation in the AFM matrix. On the other hand, spin fluctuation is suppressed under negative field. The lowest MR, positive trend under positive field and its absence under negative field, at $\theta = 45^\circ$, further support the conclusion that the AFM matrix in the sample is oriented along $\theta = 45^\circ$. The curves at 10 K [Fig. 5(d)] show a similar trend as those at 300 K, but with a stronger magnetic interaction. As a result, we observe a hysteresis in the MR curves along with an increasingly stronger positive trend as the field moves towards the in-plane direction.

The angle dependences of AsyMR and SymMR at 300 K [10 K] are shown in Figs. 5(b) and 5(c) [Figs. 5(e) and 5(f)]. We observe that the AsyMR decreases slowly till θ reaches 45° and then reduces rapidly to a slightly negative value at 90°. The AsyMR is always higher at 10 K than at 300 K for all θ 's. The SymMR curves at 300 K show a sudden drop in the resistance in the low-field region which originates from the growth of domains. The positive trend in the SymMR is more obvious for $\theta \geq 45^\circ$ at 300 K and for all θ 's at 10 K. The increase in the positive trend for in-plane direction at 300 K happens because the magnetic easy axis lies along the in-plane direction. Thus the effective magnetic field is stronger in this direction which induces a larger spin fluctuation in the AFM matrix. The positive trend at 10 K is observed for all the θ 's, because of an increase in the effective magnetic field at low temperatures.

The MR data in the high-field region are fitted with $\Delta\rho/\rho_0 = -\alpha H^n$, where α is the strength of MR. The curves are linear with $n \approx 1$, for all the measurements. There is little variation in n . The value is close to those reported for the s - d scattering [32]. We further fit the MR data with $\Delta\rho/\rho_0 = -\gamma H + \beta H^2$, and obtained $\beta/\gamma \approx 10^{-6}$, which again confirms that the behavior is almost linear in the high-field region and mostly dominated by the s - d scattering [12,29,33,34].

Angle dependent MR measurement establishes that the AsyMR is the highest when the magnetic field is applied perpendicular to the sample plane. Furthermore, all contributions show an angular dependence. Thus, we have performed the angle dependent magnetoresistance (ADMR) measurements by rotating the magnetic field in different directions to gain a better insight. We applied the magnetic field of 1, 10, and 100 kOe and measured MR as functions of angle θ , ϕ , and φ at 300 K as shown in Figs. 6(a)–6(c). The schematic of the measurement is given in Fig. 1(a). The sample displays a combination of twofold and fourfold anisotropies for all the

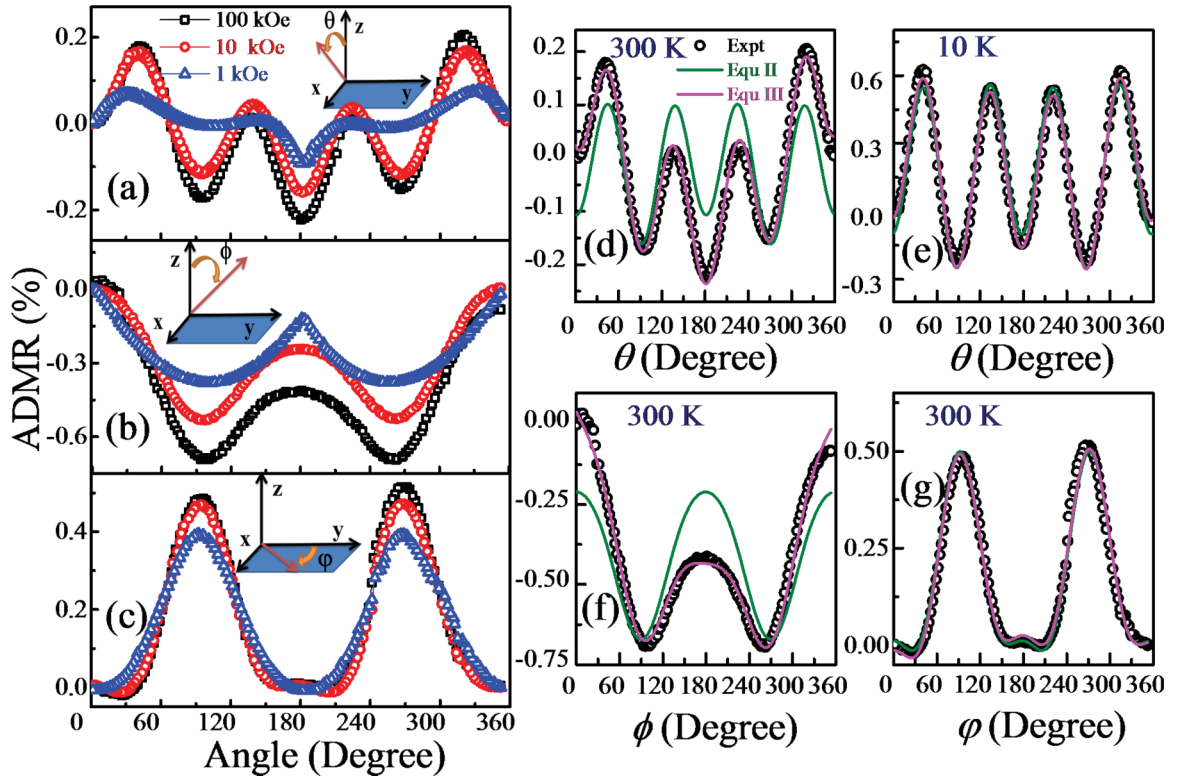


FIG. 6. Asymmetric ADMR along three orthogonal directions. (a–c) The longitudinal ADMR has been plotted as the function of the angle of magnetic field in the different directions as shown in the inset, with the current flowing in the y direction. All the ADMR curves were measured for the field of 100 (black), 10 (red), and 1 kOe (blue). Panels (d) and (e) show the ADMR for the magnetic field at an angle of θ for 300 and 10 K, respectively. Panels (f) and (g) are the AMR measured for the magnetic field at an angle of ϕ and φ , respectively. Green and magenta lines in panels (d)–(g) are curves of fitting for Eqs. (2) and (3) for θ , ϕ , and φ , respectively.

three rotations and a large asymmetry for θ and ϕ . The ADMR curve is symmetric with respect to the z axis and the asymmetry is strongest perpendicular to the sample plane. Furthermore, the asymmetry is more obvious for ϕ compared to φ . This is expected because the magnetic field points in the out-of-plane direction as ϕ increases. This measurement establishes that the asymmetry in the MR exists only along the z axis. The fourfold anisotropy in the system originates from the tetragonal phase and points to the fact that the Ni-Mn-In film is textured.

We can use a phenomenological model to describe the ADMR curves [35]. In case of a magnetically saturated crystal, the resistivity tensor is invariant with the change in magnetic field direction, thus the current density (J) is linearly proportional to electric field (E):

$$E_i = \rho_{ij} J_j. \quad (1)$$

The resistivity tensor ρ_{ij} can be determined using a series expansion in terms of direction cosine α_{ij} of the field vector up to the sixth rank, taking tetragonal crystal symmetry into consideration. The equation obtained in terms of the angle θ is given as

$$R_{XX} = C_1 + C_2 \sin(2\theta + \theta_0) + C_3 \sin(4\theta + \theta_0), \quad (2)$$

where C_1 and θ_0 are the prefactors due to the mismatch of initial conditions and C_2 and C_3 are coefficients resulting from the uniaxial and biaxial anisotropic contributions of a tetragonal phase, respectively [35].

The ADMR_θ results at 300 and 10 K for 100 kOe are fitted with Eq. (2), as shown in Figs. 6(d) and 6(e), respectively. The variation in the magnitude of uniaxial and biaxial anisotropic contributions cannot account for the observed asymmetry. The fit at 10 K is much better, as the contributions from the uniaxial and biaxial anisotropies due to crystal symmetry are stronger at lower temperatures. The AMR curves as functions of ϕ and φ (AMR_ϕ and AMR_φ) at 300 K are shown in Figs. 6(f) and 6(g). The phenomenological model predicts a similar dependence of $\text{AMR}_{\phi,\varphi}$ for ϕ and φ as in Eq. (2), but with the different prefactors and coefficients. The AMR_ϕ in Fig. 6(f) cannot be fitted with Eq. (2) for ϕ either. On the other hand, the AMR_φ curve in Fig. 6(g) fits very well with Eq. (2) for φ , showing that no asymmetry is present when the magnetic field is in plane. A large disagreement between Eq. (2) and ADMR_θ and AMR_ϕ hints at the possibility of another contribution to MR the origin of which cannot be explained in terms of crystalline anisotropies. We thus add an additional term containing $\sin(\theta/2)$ dependence to the resistance and the modified equation is given as

$$R_{XX} = C_1 + C_2 \sin(2\theta + \theta_0) + C_3 \sin(4\theta + \theta_0) + E_B \sin(\theta/2 + \theta_0), \quad (3)$$

where E_B is the coefficient of the asymmetry. This equation gives a much better fit and can account for the asymmetry in the

TABLE I. The uniaxial (C_2), biaxial (C_3), and UA prefactor (E_B) calculated by fitting with Eq. (3), ADMR_θ for 10 and 300 K, and AMR_ϕ and AMR_φ at 300 K.

Temperature (K)	C_2	C_3	E_B
10_θ	6.16×10^{-4}	36.5×10^{-4}	13.8×10^{-4}
300_θ	0.372×10^{-4}	12.4×10^{-4}	27.8×10^{-4}
300_ϕ	14.2×10^{-4}	18.3×10^{-4}	44.1×10^{-4}
300_φ	15.0×10^{-4}	24.2×10^{-4}	3.02×10^{-4}

ADMR_θ curves as seen in Figs. 6(d) and 6(e). Similarly, we add $\sin(\phi/2)$ and $\sin(\varphi/2)$ terms to the corresponding equation for ϕ and φ . The above equations for ϕ and φ are similar to Eq. (3), but with different prefactors and coefficients. Much better fits are obtained for $\text{AMR}_{\phi,\varphi}$ as shown in Figs. 6(f) and 6(g). This additional angle dependent scattering occurs because of the FM/AFM interfaces. The values of the different coefficients obtained for all the fittings are given in Table I. The ratio of the uniaxial to biaxial coefficients (C_3/C_2) is five times higher at 300 K than at 10 K for ADMR_θ . This is also evident from the large difference in the magnitude of various peaks observed in ADMR_θ curves. The ratio of the asymmetric term to biaxial term (E_B/C_3) is about six times higher at 300 K than at 10 K, even though AsyMR has comparable magnitudes as seen in Fig. 4. We observe that the uniaxial contribution to $\text{AMR}_{\phi,\varphi}$ is much larger than that of ADMR_θ . This happens because of the additional uniaxial contribution coming from the Lorentz scattering of the charge carrier [36].

IV. DISCUSSION

The uniaxial and biaxial anisotropies of the tetragonal phase gives rise to twofold and fourfold ADMR , respectively. The interaction between FM clusters and the AFM matrix results in a UA and the asymmetry in ADMR . From discussions in Secs. III A, III B, and III D, we know that the AFM matrix is randomly distributed along the surface of a cone with 45° angle and pins the FM clusters along the same direction, into the plane of the sample. The in-plane components of the FM clusters are thus randomly distributed and effectively cancel out. This results in a symmetric MR when the magnetic field rotates in plane. On the other hand, out-of-plane components add up, thus giving rise to the UA perpendicular to the film surface resulting in asymmetric MR under magnetic field along the z axis. As the sizes of the magnetic clusters are small, they do not exhibit a strong exchange coupling to show the exchange bias effect, but influence the electron scattering sensitively to give rise to the asymmetric MR [12].

When a negative magnetic field is applied at 45° angle ($\theta = 135$ and 225°), the FM clusters orient easily in the field direction. As the AFM matrix and pinned and free FM clusters are all pointing in the same direction, it results in the minimum scattering and a low-resistance state as shown in Fig. 7(a). Upon reversal of the magnetic field ($\theta = 45$ and 315°), the free FM regions rotate, which drags the pinned FM moments into a random configuration, and gives rise to a higher resistance as shown in Fig. 7(c). The frustrated moments around the

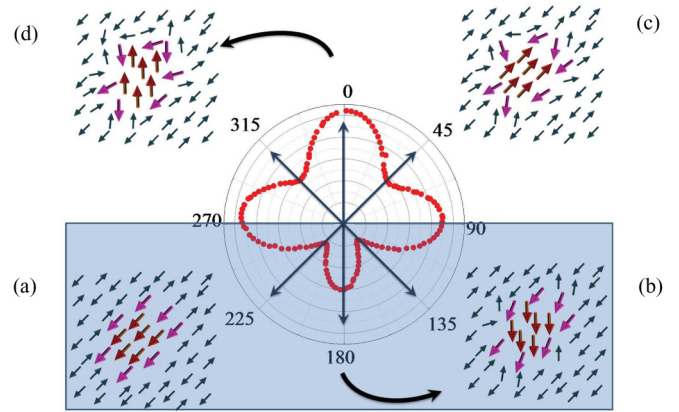


FIG. 7. Influence of the FM/AFM arrangement on the spin-valve-like MR. The blue box is the sample and the FM clusters (red arrows) are embedded in the AFM matrix (blue arrows); the surface moments (pink arrows) are pinned by the AFM matrix randomly at a 45° angle into the plane of the sample. The magnetic state of the sample at the angle $\theta = 0, 45, 180$, and 225° is shown. In the center, we have the polar ADMR_θ curve measured in the field of 100 kOe. Blue arrows on the polar graph show the easy axis and UA direction. The MR is symmetric about the z axis. The horizontal components from randomly oriented FM clusters at 45° cancel out whereas vertical contributions add up giving rise to the unidirectional anisotropy.

interfaces further introduce spin fluctuation in the adjacent AFM matrix, resulting in the positive trend in MR under a low magnetic field as observed in Fig. 5(a). This effect diminishes under higher magnetic field. Under a magnetic field at $\theta = 180^\circ$ as shown in Fig. 7(b), the magnetic clusters are oriented easily along the field direction due to the UA and the frustration caused in the pinned FM and the adjacent AFM matrix is small, resulting in a low-resistance state, whereas for the magnetic field at $\theta = 0^\circ$ the FM clusters are oriented against the UA direction. They drag the pinned FM regions into a more random configuration and cause more spin fluctuation in the surrounding AFM matrix, resulting in a maximum resistance as shown in Fig. 7(d). Further, as the magnetic field is rotated along θ , the scattering increases because the magnetic field moves away from the UA direction and maximizes when the field is opposite to the UA direction. This gives rise to the $\sin(\theta/2)$ and $\sin(\phi/2)$ terms in ADMR_θ and AMR_ϕ to account for the observed asymmetry.

In summary, we observed the SV-like effect in $\text{Ni}_{52}\text{Mn}_{40}\text{In}_8$ thin films, which remains almost constant between 10 and 400 K and is stable even under a field of 100 kOe. The SV-like MR originates from the FM/AFM interface-induced perpendicular UA, on top of the uniaxial and biaxial anisotropies of the tetragonal phase. Such an effect possesses a great potential for next generation spintronics as it is less susceptible to the perturbations. Since the magnetism of the Ni-Mn-In alloy can be tuned by changing its composition, it is expected that the UA and SV-like magnetoresistance can be further optimized. Our results open a way to achieve SV effect in many magnetic phase-separation materials where the interface between the FM and AFM phases acts as an active medium.

ACKNOWLEDGMENTS

S.A. and P.D. acknowledge support from the Chinese Academy of Sciences President's International Fellowship Initiative. We thank P. K. Mukhopadhyay for valuable suggestions. This paper was supported by the National Key Research and Development Program of China (Grants No. 2016YFA0201102 and No. 2017YFA0303602), the National Natural Science Foundation of China (Grants

No. 51571208, No. 51301191, No. 51525103, No. 11474295, and No. 51701231), the Youth Innovation Promotion Association of the Chinese Academy of Sciences (Grant No. 2016270), the Key Research Program of the Chinese Academy of Sciences (Grant No. KJZD-EW-M05), the K. C. Wong Education Foundation (Grant No. rczx0800), and the Ningbo Science and Technology Innovation Team (Grant No. 2015B11001).

-
- [1] B. Dieny, V. S. Speriosu, S. S. P. Parkin, B. A. Gurney, D. R. Wilhoit, and D. Mauri, *Phys. Rev. B* **43**, 1297 (1991).
- [2] J. S. Moodera, L. R. Kinder, T. M. Wong, and R. Meservey, *Phys. Rev. Lett.* **74**, 3273 (1995).
- [3] S. S. P. Parkin, N. More, and K. P. Roche, *Phys. Rev. Lett.* **64**, 2304 (1990).
- [4] D. H. Mosca, F. Petroff, A. Fert, P. A. Schroeder, W. P. Pratt, and R. Laloe, *J. Magn. Magn. Mater.* **94**, L1 (1991).
- [5] C. Chappert, A. Fert, and F. N. Van Dau, *Nat. Mater.* **6**, 813 (2007).
- [6] L. Néel, *Nobel Lectures, Physics 1963–1970* (Elsevier, Amsterdam, 1972).
- [7] R. Y. Umetsu, A. Sakuma, and K. Fukamichi, *Appl. Phys. Lett.* **89**, 052504 (2006).
- [8] T. Jungwirth, X. Marti, P. Wadley, and J. Wunderlich, *Nat. Nanotechnol.* **11**, 231 (2016).
- [9] P. Wadley, B. Howells, J. Elezny, C. Andrews, V. Hills, R. P. Campion, V. Novak, K. Olejnik, F. Maccherozzi, S. S. Dhesi, S. Y. Martin, T. Wagner, J. Wunderlich, F. Freimuth, Y. Mokrousov, J. Kune, J. S. Chauhan, M. J. Grzybowski, A. W. Rushforth, K. W. Edmonds, B. L. Gallagher, and T. Jungwirth, *Science* **351**, 587 (2016).
- [10] X. Marti, I. Fina, C. Frontera, J. Liu, P. Wadley, Q. He, R. J. Paull, J. D. Clarkson, J. Kudrnovský, I. Turek, J. Kuneš, D. Yi, J. H. Chu, C. T. Nelson, L. You, E. Arenholz, S. Salahuddin, J. Fontcuberta, T. Jungwirth, and R. Ramesh, *Nat. Mater.* **13**, 367 (2014).
- [11] B. G. Park, J. Wunderlich, X. Martí, V. Holý, Y. Kurosaki, M. Yamada, H. Yamamoto, A. Nishide, J. Hayakawa, H. Takahashi, A. B. Shick, and T. Jungwirth, *Nat. Mater.* **10**, 347 (2011).
- [12] S. Singh, R. Rawat, S. E. Muthu, S. W. D'Souza, E. Suard, A. Senyshyn, S. Banik, P. Rajput, S. Bhardwaj, A. M. Awasthi, R. Ranjan, S. Arumugam, D. L. Schlagel, T. A. Lograsso, A. Chakrabarti, and S. R. Barman, *Phys. Rev. Lett.* **109**, 246601 (2012).
- [13] K. P. Bhatti, S. El-Khatib, V. Srivastava, R. D. James, and C. Leighton, *Phys. Rev. B* **85**, 134450 (2012).
- [14] S. Yuan, P. L. Kuhns, A. P. Reyes, J. S. Brooks, M. J. R. Hoch, V. Srivastava, R. D. James, S. El-Khatib, and C. Leighton, *Phys. Rev. B* **91**, 214421 (2015).
- [15] B. M. Wang, Y. Liu, P. Ren, B. Xia, K. B. Ruan, J. B. Yi, J. Ding, X. G. Li, and L. Wang, *Phys. Rev. Lett.* **106**, 077203 (2011).
- [16] B. M. Wang, Y. Liu, L. Wang, S. L. Huang, Y. Zhao, Y. Yang, and H. Zhang, *J. Appl. Phys.* **104**, 043916 (2008).
- [17] T. Krenke, M. Acet, E. F. Wassermann, X. Moya, L. Mañosa, and A. Planes, *Phys. Rev. B* **72**, 014412 (2005).
- [18] T. Krenke, M. Acet, E. F. Wassermann, X. Moya, L. Mañosa, and A. Planes, *Phys. Rev. B* **73**, 174413 (2006).
- [19] D. Pravarthana, D. Chateigner, L. Lutterotti, M. Lacotte, S. Marinell, P. A. Dubos, I. Hervas, E. Hug, P. A. Salvador, and W. Prellier, *J. Appl. Phys.* **113**, 153510 (2013).
- [20] K. Yoshida, T. Ishizaka, M. Kuroda, and S. Ikawa, *Acta Mater.* **55**, 4499 (2007).
- [21] J. K. Mason and C. A. Schuh, in *Electron Backscatter Diffraction in Materials Science* (Springer, New York, 2009), pp. 35–51.
- [22] C. Zeng, Y. Yao, Q. Niu, and H. H. Weitering, *Phys. Rev. Lett.* **96**, 037204 (2006).
- [23] B. P. de Laune, F. J. Berry, J. F. Marco, S. L. Horswell, and C. Greaves, *J. Mater. Chem. C* **4**, 5320 (2016).
- [24] J. S. Kasper and J. S. Kouvel, *J. Phys. Chem. Solids* **11**, 231 (1959).
- [25] L. Pál, E. Krén, G. Kádár, P. Szabó, and T. Tarnóczy, *J. Appl. Phys.* **39**, 538 (1968).
- [26] W. L. O'Brien and B. P. Tonner, *Phys. Rev. B* **51**, 617 (1995).
- [27] R. H. Yu, X. X. Zhang, J. Tejada, and J. Zhu, *Phys. Rev. B* **52**, R6987(R) (1995).
- [28] A. N. Dobrynin, D. N. Ievlev, K. Temst, P. Lievens, J. Margueritat, J. Gonzalo, C. N. Afonso, S. Q. Zhou, A. Vantomme, E. Piscopiello, and G. Van Tendeloo, *Appl. Phys. Lett.* **87**, 012501 (2005).
- [29] S. Banik, R. Rawat, P. K. Mukhopadhyay, B. L. Ahuja, A. Chakrabarti, P. L. Paulose, S. Singh, A. K. Singh, D. Pandey, and S. R. Barman, *Phys. Rev. B* **77**, 224417 (2008).
- [30] M. Kataoka, *Phys. Rev. B* **63**, 134435 (2001).
- [31] S. Singh, I. Glavatsky, and C. Biswas, *J. Alloys Compd.* **615**, 994 (2014).
- [32] C. Jing, Y. Yang, X. Wang, P. Liao, D. Zheng, B. Kang, S. Cao, J. Zhang, J. Zhu, and Z. Li, *Prog. Nat. Sci. Mater. Int.* **24**, 19 (2014).
- [33] P. Dutta, S. Pramanick, V. Singh, D. T. Major, D. Das, and S. Chatterjee, *Phys. Rev. B* **93**, 134408 (2016).
- [34] S. Singh and C. Biswas, *Appl. Phys. Lett.* **98**, 212101 (2011).
- [35] J. Li, S. L. Li, Z. W. Wu, S. Li, H. F. Chu, J. Wang, Y. Zhang, H. Y. Tian, and D. N. Zheng, *J. Phys.: Condens. Matter* **22**, 146006 (2010).
- [36] A. Annadi, Z. Huang, K. Gopinadhan, X. R. Wang, A. Srivastava, Z. Q. Liu, H. H. Ma, T. P. Sarkar, T. Venkatesan, and Ariando, *Phys. Rev. B* **87**, 201102 (2013).